

Spin relaxation mechanism in graphene: resonant scattering by magnetic impurities

Denis Kochan, Martin Gmitra, and Jaroslav Fabian
*Institute for Theoretical Physics, University of Regensburg,
 93040 Regensburg, Germany*

(Dated: February 25, 2022)

It is proposed that the observed small (100 ps) spin relaxation time in graphene is due to resonant scattering by local magnetic moments. At resonances, magnetic moments behave as spin hot spots: the spin-flip scattering rates are as large as the spin-conserving ones, as long as the exchange interaction is greater than the resonance width. Smearing of the resonance peaks by the presence of electron-hole puddles gives quantitative agreement with experiment, for about 1 ppm of local moments. While the local moments can come from a variety of sources, we specifically focus on hydrogen adatoms. We perform first-principles supercell calculations and introduce an effective Hamiltonian to obtain realistic input parameters for our mechanism.

Graphene [1, 2] has been considered an ideal spintronics [3, 4] material. Its spin-orbit coupling being weak, the spin lifetimes of Dirac electrons are expected to be long, on the order of microseconds [5]. Yet experiments find tenths of a nanosecond [6–13]. This vast discrepancy has been the most outstanding puzzle of graphene spintronics. Despite intense theoretical efforts [14–21], the mechanism for the spin relaxation in graphene has remained elusive. Recently, mesoscopic transport experiments [22] found evidence that local magnetic moments could be the culprits. Here we propose a mechanism of how even a small concentration of such moments can drastically reduce the spin lifetime of Dirac electrons. If the local moments sit at resonant scatterers, such as vacancies [23–25] and adatoms [25, 26], they can act as spin hot spots [27]: while contributing little to momentum relaxation, they can dominate spin relaxation. Although our mechanism is general, we specifically assume that local moments come from hydrogen adatoms. The calculated spin relaxation rates for 1 ppm of local moments, when averaged over electron density fluctuations due to electron-hole puddles, are in quantitative agreement with experiment. Our theory shows that in order to increase the spin lifetime in graphene, local magnetic moments at resonant scatterers need to be chemically isolated or otherwise eliminated.

Magnetic impurities typically do not play a role in the electron spin relaxation of conductors [3], unless when doped with transition metal elements. In graphene the presence of local magnetic moments is not obvious, unless the magnetic sites (vacancies or adatoms) are intentionally produced [24, 25]. It is reasonable to expect that there are not more magnetic sites than, say, 1 ppm, in graphene samples investigated for spin relaxation. For this concentration a simple estimate gives a weak spin relaxation rate, similar to what is predicted for spin-orbit coupling mechanisms. Indeed, the Fermi golden rule gives, for exchange coupling J between electrons and local moments, spin relaxation rate $1/\tau_s \approx \frac{2\pi}{\hbar} \eta J^2 \nu_0(E_F)$, where $\nu_0(E_F)$ is graphene's density of states at the Fermi

level and η is the concentration of the moments. Taking representative values of $J \approx 0.4$ eV, $\eta \approx 10^{-6}$, and $E_F \approx 0.1$ eV (for which ν_0 is about 0.01 states per eV and atom), one gets spin relaxation times of 100 ns, three orders below the experimental 100 ps.

What we show in this paper is that the spin relaxation due to magnetic impurities in graphene is significantly enhanced by resonant scattering, for which the perturbative Fermi golden rule does not apply. The intuitive idea is that if the exchange coupling J is greater than the resonance width Γ , the electron spin can precess at resonance by at least one period during the interaction time with the impurity. Then the spin-flip probability becomes as likely as the spin-conserving one. This idea is confirmed by an explicit calculation for graphene with a hydrogen adatom. We use a supercell first-principles band structure to investigate the local magnetic moments (as has been done earlier [26]) and parameterize the band structure in terms of effective exchange couplings, to obtain their realistic estimates. We then use a single impurity spin model with exchange on the resonance site to calculate the T-matrix and spin relaxation rate. Finally, we illustrate the intuitive picture of resonant spin enhancement on a toy one-dimensional model of an electron scattering off a magnetic moment in a resonant quantum well.

Spin-polarized band structure of hydrogenated graphene. The electronic structure of a relaxed 5×5 supercell with a single H atom on top of a C atom (denoted below as C_H) has been calculated within density functional theory using the full-potential linearized augmented plane wave method as implemented in the FLEUR code [28]. Figure 1(a-f) shows the results. The valence and conduction bands are separated at K point due to covalent bonding of carbon p_z and hydrogen s orbitals by about 1 eV. In between lies the mid-gap band formed mainly by p_z orbitals of C atoms closest to H. The ground state is ferromagnetic, with the exchange splitting of about 0.1 eV. The magnetic moment is significant in a close neighborhood of C_H

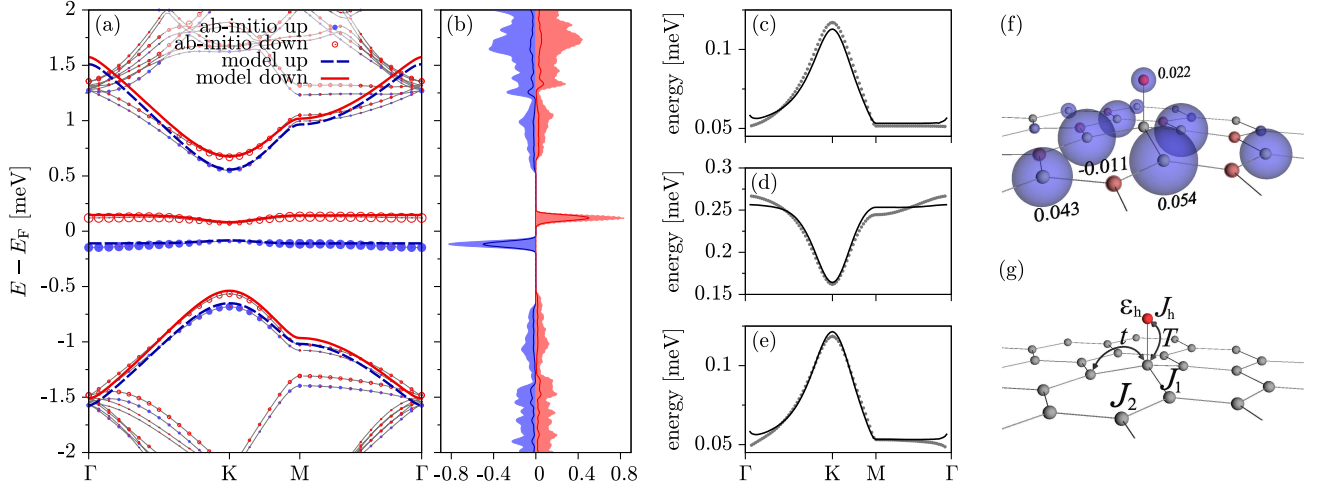


FIG. 1. First-principles results for a 5×5 graphene supercell with a single hydrogen adatom. (a) Spin-polarized band structure. The circles radii indicate the presence of p_z orbitals from the nearest neighbors to C_H . Bold lines (dashed and solid) come from the exchange hopping model, Eq. (1). (b) Total density of states per atom (filled) and p_z projected local densities summed up to the third nearest carbon atoms to C_H , normalized to the corresponding number of atoms in the set. Exchange splittings of the conduction (c), mid-gap (d), and valence (e) bands. Solid lines are from the model. (f) Local magnetic moments around hydrogen, indicated in μ_B . (g) Exchange hopping model of Eq. (1).

only, oscillating as a function of position. The largest moment, of $0.054 \mu_B$, is on the nearest neighbors to C_H . Hence the spin splitting of the mid-gap states is maximal and gradually decreases for the bands away from the Fermi level, whose character is less influenced by the H region.

To parameterize the first-principles data, we have extended the hopping Hamiltonian studied in Refs. [29–31]. The scheme is in Fig. 1(g). The orbital effects due to H are captured by on-site energy ε_h and hopping T . To this we add model exchange couplings J_h , J_1 and J_2 , on the sites of large magnetic moments, inspired by Fig. 1(f). The impurity Hamiltonian H'_{eff} , which is added to graphene's $H_0 = -t \sum_{\langle m,n \rangle} c_m^\dagger c_n$ ($t = 2.6 \text{ eV}$) is

$$H'_{\text{eff}} = \sum_{\sigma} h_{\sigma}^{\dagger} (\varepsilon_h - J_h \hat{\sigma}_z) h_{\sigma} + T (h_{\sigma}^{\dagger} c_{C_H, \sigma} + c_{C_H, \sigma}^{\dagger} h_{\sigma}) - J_1 \sum_{m_1, \sigma} c_{m_1, \sigma}^{\dagger} \hat{\sigma}_z c_{m_1, \sigma} - J_2 \sum_{m_2, \sigma} c_{m_2, \sigma}^{\dagger} \hat{\sigma}_z c_{m_2, \sigma}. \quad (1)$$

Here h_{σ}^{\dagger} (h_{σ}) and c_{σ}^{\dagger} (c_{σ}) are fermionic creation (annihilation) operators acting on the hydrogen and graphene carbon sites, respectively. Subscript $\sigma = \{\uparrow, \downarrow\}$ stands for the spin component along the z -direction (quantization axis); $\hat{\sigma}_z$ is the Pauli matrix. Subscripts m_1 and m_2 label the three first-nearest and the six second-nearest neighbors of C_H .

Orbital parameters $\varepsilon_h = 0.16 \text{ eV}$ and $T = 7.5 \text{ eV}$ were fitted already in Ref. [31]. Least-square fitting the model Hamiltonian H'_{eff} , Eq. (1), to our supercell spin-polarized first-principles data, gives $J_h = -0.82 \text{ eV}$, $J_1 = 0.69 \text{ eV}$, and $J_2 = -0.18 \text{ eV}$. We fitted the valence, mid-gap, and conduction bands at 100 equidistant points along ΓKMF .

The fits, shown in Fig. 1(a) and detailed in Fig. 1(c-e), are remarkably good especially around K. We find that J_h alone controls the exchange splitting of the valence and conduction bands in a large region around K point.

Resonant scattering by magnetic impurities. To solve the magnetic scattering problem using H'_{eff} in the single impurity limit is numerically demanding. However, the most important spin-flip contribution is expected to come from the exchange coupling on the resonant scatterer (H atom) site [32]. We thus neglect J_1 and J_2 terms and propose the reduced Hamiltonian, $H'(\hat{\mathbf{S}})$:

$$H'(\hat{\mathbf{S}}) = \sum_{\sigma} \varepsilon_h h_{\sigma}^{\dagger} h_{\sigma} + T (h_{\sigma}^{\dagger} c_{C_H, \sigma} + c_{C_H, \sigma}^{\dagger} h_{\sigma}) - J \hat{\mathbf{S}} \cdot \hat{\mathbf{S}}. \quad (2)$$

The exchange term describes the interaction of electron spin $\hat{\mathbf{s}} = h_{\alpha}^{\dagger} \hat{\boldsymbol{\sigma}}_{\alpha\beta} h_{\beta}$ and impurity moment $\hat{\mathbf{S}}$. We keep orbital parameters $\varepsilon_h = 0.16 \text{ eV}$ and $T = 7.5 \text{ eV}$, and take a generic value $J = -0.4 \text{ eV}$ for exchange. The spin relaxation rates, when broadened by puddles, are hardly influenced by the precise value and the sign of J [32].

In the independent electron-impurity picture (we do not discuss Kondo physics), total Hamiltonian $H_0 + H'(\hat{\mathbf{S}})$ diagonalizes in the singlet ($\ell = 0$) and triplet ($\ell = 1$) basis $|\ell, m_{\ell}\rangle$ (here m_{ℓ} runs from $-\ell$ to ℓ). Eliminating by downfolding (Löwdin transformation) H orbitals, we arrive at the single-site impurity Hamiltonian,

$$H'_{\text{fold}}(\hat{\mathbf{S}}) = \sum_{\ell, m_{\ell}} \alpha_{\ell}(E) c_{C_H, \ell, m_{\ell}}^{\dagger} c_{C_H, \ell, m_{\ell}}, \quad (3)$$

where the energy-dependent on-site coupling is,

$$\alpha_{\ell}(E) = \frac{T^2}{E - \varepsilon_h + (4\ell - 3)J}, \quad (4)$$

different for singlet and triplet states.

The T-matrix elements for the above impurity problem can be calculated as (see, e. g., [33])

$$T(E)_{\kappa',\ell',m_{\ell'}|\kappa,\ell,m_{\ell}} = \frac{1}{N_C} \frac{\delta_{\ell,\ell'} \delta_{m_{\ell},m_{\ell'}} \alpha_{\ell}(E)}{1 - \alpha_{\ell}(E)G_0(E)}. \quad (5)$$

where κ labels momentum and band index of graphene's Bloch states, N_C is the number of carbon sites in the sample, and $G_0(E)$ is the retarded Green function per carbon atom and spin of unperturbed graphene. Near the neutrality point ($E = 0$), $G_0(E) \simeq \frac{E}{D^2} [\ln |\frac{E^2}{D^2 - E^2}| - i\pi \text{sgn}(E)\Theta(D - |E|)]$, where the graphene bandwidth $D = \sqrt{3}\pi t \approx 6 \text{ eV}$.

Resonant states appear for energies $|E| < D$ at which the real part of the denominator of Eq. (5) equals zero. Near the neutrality point ($|E| \ll D$) we get the equation

$$E_{\text{res},\ell} \left(1 - \frac{T^2}{D^2} \ln \frac{E_{\text{res},\ell}^2}{D^2} - \frac{T^2}{D^4} E_{\text{res},\ell}^2 \right) = \varepsilon_h - (4\ell - 3)J \quad (6)$$

which determines the resonant energies $E_{\text{res},\ell}$ for singlet and triplet states. For a non-magnetic impurity ($J = 0$) there appears a single resonant level close to the neutrality point [30]. For a magnetic impurity this level splits to singlet and triplet peaks, and shifts in energy. For $J < 0$ the singlet resonance has a lower energy, see [32].

From the T-matrix we obtain spin-flip rate $1/\tau_s$ at zero temperature (thermal broadening is discussed in [32]),

$$1/\tau_s = \eta \frac{2\pi}{\hbar} \nu_0(E) f_{-\sigma,\sigma} \left(\frac{\alpha_1(E)}{1 - \alpha_1 G_0(E)}, \frac{\alpha_0(E)}{1 - \alpha_0 G_0(E)} \right), \quad (7)$$

for the fraction of $\eta = N_A/N_C$ of impurities per carbon atom. Couplings $\alpha_{\ell}(E)$ are given by Eq. (4), $G_0(E)$ and $\nu_0(E)$ are graphene's Green function and DOS per atom and spin, and auxiliary function $f_{\sigma,\sigma'}(x, y)$ is,

$$f_{\sigma,\sigma'}(x, y) = \frac{1}{2} \delta_{\sigma,\sigma'} |x|^2 + \frac{1}{8} |x + (\sigma \cdot \sigma') y|^2. \quad (8)$$

The spin-flip rate $1/\tau_s$ is peaked at resonances where denominators $1 - \alpha_{\ell}(E)G_0(E)$ have minima.

Spin relaxation rate $1/\tau_s$ is plotted in Fig. 2, which is the main result of this paper. Zero temperature rate shows singlet and triplet split resonance peaks, with widths Γ of about 20 and 40 meV, respectively. At 300 K the peaks merge. In realistic samples the neutrality point fluctuates due to electron-hole puddles [34, 35]. Also, different magnetic impurities would give different peak positions and widths, providing additional broadening. All such effects are modeled by gaussian energy broadening with standard deviation σ_{br} . In Fig. 2 we use $\sigma_{\text{br}} = 110 \text{ meV}$. From Fig. 2(b) we can conclude that the temperature dependence of $1/\tau_s$ is rather weak, essentially given by Fermi broadening of the resonance structure. Finally, in Fig. 2(c) we compare the calculated spin relaxation rates with experiment, with adjusted η . The

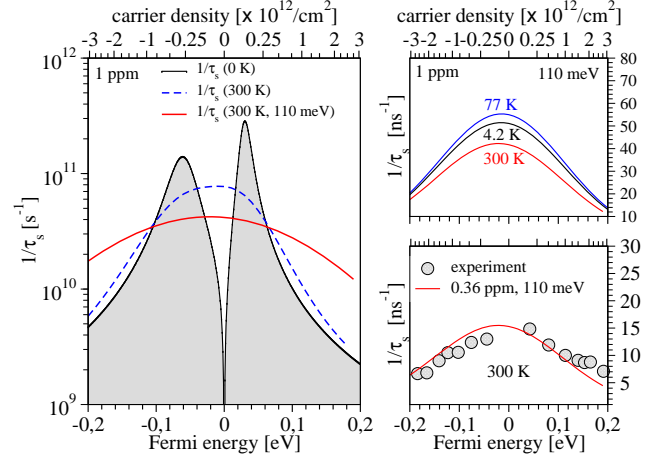


FIG. 2. Resonant enhancement of spin relaxation in graphene. Exchange $J = -0.4 \text{ eV}$ and impurity fraction η is indicated. (a) Spin relaxation rate $1/\tau_s$ as a function of energy/carrier density, at 0 K, at 300 K, and at 300 K broadened by puddles with energy fluctuations of 110 meV. (b) Broadened $1/\tau_s$ at different T . (c) Comparison between theory and experiment (graphene data from Ref. [36]) at 300 K.

agreement is remarkable. In fact, one can find a nice agreement for a large window of J (see [32]) by adjusting σ_{br} and η . Vacancies and different adatoms are well covered by this mechanism.

In [32] we plot $1/\tau_s$ for ferromagnetic $J = 0.4 \text{ eV}$. The only effect, after broadening, is the opposite (slight) skewness of the energy dependence (keeping ε_h unchanged), coming from the flipped positions of the singlet and triplet peaks. Also, in [32] we demonstrate that resonance enhancement of $1/\tau_s$ is present for even much smaller J , as long as $J \gtrsim \Gamma$, confirming the intuitive picture of the enhancement coming from the spin precession being faster than the leakage rate. One important conclusion one can draw from this concerns spin-orbit coupling (SOC). Hydrogen adatoms induce SOC of about 1 meV [31, 37]. This is smaller than Γ , so the resonant enhancement will be much less pronounced, unless η is increased to, say 10^{-3} [32]. Nevertheless, there could be heavier adatoms that induce both large spin-orbit coupling and resonant scattering so that resonance enhancement could be present. It was recently shown that Si adatoms sitting on top of the carbon bonds could also give 100 ps spin-flip times [21], but for concentrations of $\eta \sim 10^{-3}$, three orders more than what is needed for magnetic resonant scatterers. It is possible that the mechanism is indeed resonance enhancement of the spin-flip rates. In fact, resonant scattering by spin-orbit coupling inducing impurities was already invoked to explain strong spin-flip scattering in alkali [38] and noble [39] metals.

There have already been spin relaxation experiments with hydrogenated graphene. According to our theory,

an sp^3 bonded hydrogen should increase the spin relaxation rate. Unfortunately, the experimental results differ. In Ref. [36] the spin relaxation rate decreased upon hydrogenation. In Ref. [37] spin relaxation has not changed much, while in Ref. [25] evidence for magnetic moments was provided based on a different model, that of fluctuating magnetic fields. It is likely that the experimental outcomes depend on the hydrogenation method. At present it is not possible to form a unique experimental picture with which we could gauge our theory. But we stress that we use hydrogen only as a convenient model to formulate our mechanism quantitatively. The Hamiltonian we use is rather generic, and the results are very robust as far as the details in J and other parameters are concerned. It is even possible that hydrogenation isolates existing magnetic moments at vacancies, thereby increasing τ_s , as seen in Ref. [36].

Resonant spin-flip scattering in a one-dimensional double-barrier atomic chain. To make the resonant enhancement of the spin relaxation rate more transparent, we introduce a toy model that captures all the essential features. Consider an atomic chain with lattice constant b , whose central site ($m = 0$), trapped within two δ barriers on its nearest neighbors, hosts the exchange interaction $J\hat{\mathbf{s}} \cdot \hat{\mathbf{S}}$. The hopping Hamiltonian is

$$H = -t \sum_{\langle m,n \rangle} (c_m^\dagger c_n + c_n^\dagger c_m) + U \sum_{m=\mp 1} c_m^\dagger c_m - J\hat{\mathbf{s}} \cdot \hat{\mathbf{S}}, \quad (9)$$

as sketched in the inset of Fig. 3(a). In the singlet-triplet basis the transmission and reflection amplitudes $\gamma_{\ell, m_\ell}(k)$ and $\beta_{\ell, m_\ell}(k)$, are obtained analytically as

$$\gamma_{\ell, m_\ell}(k) = \frac{2it(1 + Ue^{ikb}/t)^{-1} \sin kb}{[E_k + J(4\ell - 3)](1 + Ue^{ikb}/t) + 2te^{ikb}}, \quad (10)$$

$$\beta_{\ell, m_\ell}(k) = \gamma_{\ell, m_\ell}(k) - \frac{t + Ue^{-ikb}}{t + Ue^{ikb}}. \quad (11)$$

The energy of the incident electron of momentum k is $E_k = -2t \cos(kb)$, and the composite (electron and impurity) spin state $|\ell, m_\ell\rangle$, with angular momentum $\ell = 1$ for triplet and $\ell = 0$ for singlet states; m_ℓ is the corresponding angular momentum projection (this index is dropped in what follows, as neither amplitude depends on it). We are interested in the transmission $t = |\gamma|^2$ and reflection $r = |\beta|^2$ probabilities of various spin transition processes $\sigma \rightarrow \sigma'$ so we trace out the impurity spin. The result is

$$t(E_k)_{\sigma, \sigma'} = f_{\sigma, \sigma'}(\gamma_1(k), \gamma_0(k)), \quad (12)$$

$$r(E_k)_{\sigma, \sigma'} = f_{\sigma, \sigma'}(\beta_1(k), \beta_0(k)), \quad (13)$$

where function $f_{\sigma, \sigma'}$ is given by Eq. (8). The above results are shown in Fig. 3(a). We plot the ratio $\mathcal{R}(E)$ of spin flip *versus* spin-conserving probabilities $\mathcal{R}(E) =$

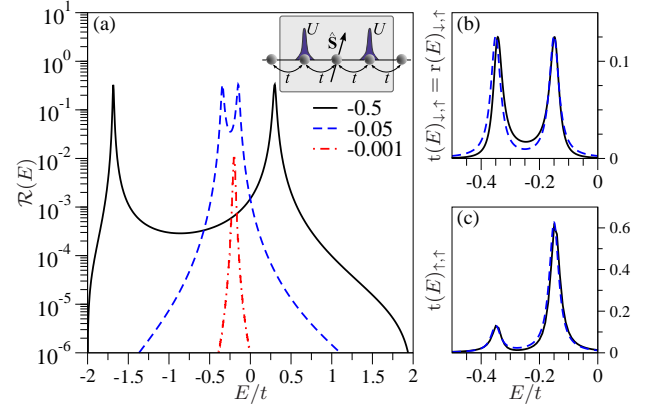


FIG. 3. Resonant enhancement of spin flips in a one dimensional atomic chain with a double barrier hosting an impurity spin. (a) Ratio $\mathcal{R}(E)$ of spin-flip and spin-conserving transition probabilities for $U/t = 10$ and indicated J/t . Inset shows the model. (b) Spin-flip $t(E)_{\downarrow, \uparrow}$ and (c) spin-conserving $t(E)_{\uparrow, \uparrow}$ probabilities for $J/t = -0.05$. The solid lines are exact formulas, Eqs. (12)-(13), the dashed lines are approximations, Eq. (14).

$[t(E)_{\sigma, -\sigma} + r(E)_{\sigma, -\sigma}] / [t(E)_{\sigma, \sigma} + r(E)_{\sigma, \sigma}]$ for different J/t . For $J/t = -0.5$ and -0.05 , i. e., when $t^2/U^2 \lesssim J/t$, spin-flip transitions are as likely as the spin-conserving ones. For smaller J/t , spin-flip probabilities become proportional to J^2 , reaching the usual perturbative regime.

Pronounced resonances appear for $U \gg t$. In this limit the singlet and triplet resonant energies are $E_{\text{res}, \ell} \simeq -2t^2/U - J(4\ell - 3)$, and $\Gamma \simeq t^3/4U^2$ is the resonance width. The dwell time $\Delta t_{\text{dw}} = \hbar/\Gamma$ is much greater than the hopping time \hbar/t . We further assume that $\Gamma \lesssim J$, which is the limit of resonant enhancement of spin relaxation rate. This condition means that the electron has enough time to precess by the exchange field before leaking out of the well. The singlet and triplet resonance peaks are well resolved in this limit. Equation (12) now gives Lorentzian,

$$t(E)_{\sigma, \sigma'} \simeq \sum_{\ell=0,1} \frac{(4\ell\delta_{\sigma, \sigma'} + 1)t^6/2U^4}{(E - E_{\text{res}, \ell})^2 + 4t^6/U^4}, \quad (14)$$

and similarly Eq. (13) the reflectivities; $r_{\sigma, -\sigma} = t_{\sigma, -\sigma}$, and $r_{\sigma, \sigma} = 1 - r_{\sigma, -\sigma} - t_{\sigma, \sigma} - t_{\sigma, -\sigma}$. Figures 3(b) and 3(c) show the comparison of the exact and above approximative formulas for $J/t = -0.05$. The peak positions depend on J via $E_{\text{res}, \ell}$, but the values at maxima are J -independent. At resonances the spin-flip to spin-conserving probabilities come as $1/3$, see Fig. 3(a): 25% of scattered electrons change spin. The reason is that a spin up electron forms triplet state $|1, 1\rangle$ with 50% chance, $|1, 0\rangle$ and $|0, 0\rangle$ with 25%. The chance that the electron flips its spin is 50% for each $|1, 0\rangle$ and $|0, 0\rangle$ states. This gives the 25% probability for a spin-flip, as we see at resonances.

In [32] we show, using our 1d model, that an impurity sitting at the barrier site and not inside the well, does not have such a pronounced effect on the spin-flip probability, justifying our exchange model of hydrogen on graphene that places J on the hydrogen site only.

In conclusion, we propose that resonant scattering by magnetic impurities in graphene, caused by vacancies or adatoms, causes the observed fast spin relaxation rates. Resonant enhancement of exchange interaction, but also of the weaker spin-orbit coupling, opens new prospects for investigating impurity magnetic moments, dynamical polarization of impurity spins, Kondo physics, and resonant scattering in graphene.

We thank T. Wehling for useful discussions, T. Maassen for providing us the experimental data to Fig. 2, and P. Mavropoulos for useful discussions and for pointing to us Ref. [38]. This work was supported by the DFG SFB 689 and SPP 1285.

-
- [1] A. K. Geim and K. S. Novoselov, *Nat. Materials* **6**, 183 (2007).
 - [2] A. H. Castro Neto, *Science* **332**, 315 (2011).
 - [3] I. Žutić, J. Fabian, and S. Das Sarma, *Rev. Mod. Phys.* **76**, 323 (2004).
 - [4] J. Fabian, A. Matos-Abiad, C. Ertler, P. Stano, and I. Žutić, *Acta Phys. Slovaca* **57**, 565 (2007).
 - [5] D. Pesin and A. H. MacDonald, *Nat. Materials* **11**, 409 (2012).
 - [6] N. Tombros, C. Józsa, M. Popinciuc, H. T. Jonkman, and B. J. van Wees, *Nature* **448**, 571 (2007).
 - [7] N. Tombros, S. Tanabe, A. Veligura, C. Józsa, M. Popinciuc, H. T. Jonkman, and B. J. van Wees, *Phys. Rev. Lett.* **101**, 046601 (2008).
 - [8] K. Pi, W. Han, K. M. McCreary, A. G. Swartz, Y. Li, and R. K. Kawakami, *Phys. Rev. Lett.* **104**, 187201 (2010).
 - [9] T.-Y. Yang, J. Balakrishnan, F. Volmer, A. Avsar, M. Jaiswal, J. Samm, S. R. Ali, A. Pachoud, M. Zeng, M. Popinciuc, G. Güntherodt, B. Beschoten, and B. Özyilmaz, *Phys. Rev. Lett.* **107**, 047206 (2011).
 - [10] W. Han and R. K. Kawakami, *Phys. Rev. Lett.* **107**, 047207 (2011).
 - [11] A. Avsar, T.-Y. Yang, S. Bae, J. Balakrishnan, F. Volmer, M. Jaiswal, Z. Yi, S. R. Ali, G. Guntherodt, B. H. Hong, B. Beschoten, and B. Özyilmaz, *Nano Letters* **11**, 2363 (2011).
 - [12] S. Jo, D.-K. Ki, D. Jeong, H.-J. Lee, and S. Kettemann, *Phys. Rev. B* **84**, 075453 (2011).
 - [13] R. G. Mani, J. Hankinson, C. Berger, and W. A. de Heer, *Nature Commun.* **3**, 996 (2012).
 - [14] D. Huertas-Hernando, F. Guinea, and A. Brataas, *Phys. Rev. B* **74**, 155426 (2006).
 - [15] B. Dora, F. Muranyi, and F. Simon, *Eur. Phys. Lett.* **92**, 17002 (2010).
 - [16] J.-S. Jeong, J. Shin, and H.-W. Lee, *Phys. Rev. B* **84**, 195457 (2011).
 - [17] V. K. Dugaev, E. Y. Sherman, and J. Barnaś, *Phys. Rev. B* **83**, 085306 (2011).
 - [18] C. Ertler, S. Konschuh, M. Gmitra, and J. Fabian, *Phys. Rev. B* **80**, 041405 (2009).
 - [19] P. Zhang and M. W. Wu, *Phys. Rev. B* **84**, 045304 (2011).
 - [20] H. Ochoa, A. H. Castro Neto, and F. Guinea, *Phys. Rev. Lett.* **108**, 206808 (2012).
 - [21] D. V. Fedorov, M. Gradhand, S. Ostanin, I. V. Maznichenko, A. Ernst, J. Fabian, and I. Mertig, *Phys. Rev. Lett.* **110**, 156602 (2013).
 - [22] M. B. Lundberg, R. Yang, J. Renard, and J. A. Folk, *Phys. Rev. Lett.* **110**, 156601 (2013).
 - [23] M. M. Ugeda, I. Brihuega, F. Guinea, and J. M. Gomez-Rodriguez, *Phys. Rev. Lett.* **104**, 096804 (2010).
 - [24] R. R. Nair, M. Sepioni, I. L. Tsai, O. Lehtinen, J. Keinonen, A. V. Krasheninnikov, T. Thomson, A. K. Geim, and I. V. Grigorieva, *Nature Physics* **8**, 199 (2012).
 - [25] K. M. McCreary, A. G. Swartz, W. Han, J. Fabian, and R. K. Kawakami, *Phys. Rev. Lett.* **109**, 186604 (2012).
 - [26] O. Yazyev, *Rep. Prog. Phys.* **73**, 056501 (2010).
 - [27] J. Fabian and S. Das Sarma, *Phys. Rev. Lett.* **81**, 5624 (1998).
 - [28] See <http://www.flapw.de/>.
 - [29] J. P. Robinson, H. Schomerus, L. Oroszlány, and V. I. Fal'ko, *Phys. Rev. Lett.* **101**, 196803 (2008).
 - [30] T. O. Wehling, S. Yuan, A. I. Lichtenstein, A. K. Geim, and M. I. Katsnelson, *Phys. Rev. Lett.* **105**, 056802 (2010).
 - [31] M. Gmitra, D. Kochan, and J. Fabian, “Spin-orbit coupling in hydrogenated graphene,” *Phys. Rev. Lett.* (in press), arXiv: 1303.2806.
 - [32] See Supplemental Material for details.
 - [33] A. C. Hewson, *The Kondo Problem to Heavy Fermions* (Cambridge University Press, Cambridge, GB, 1993).
 - [34] E. H. Hwang, S. Adam, and S. Das Sarma, *Phys. Rev. Lett.* **98**, 186806 (2007).
 - [35] A. Deshpande, W. Bao, F. Miao, C. N. Lau, and B. J. LeRoy, *Phys. Rev. B* **79**, 205411 (2009).
 - [36] M. Wojtaszek, I. J. Vera-Marun, T. Maassen, and B. J. van Wees, *Phys. Rev. B* **87**, 081402 (2013).
 - [37] J. Balakrishnan, G. K. W. Koon, M. Jaiswal, A. H. Castro Neto, and B. Özyilmaz, *Nature Physics* **9**, 284 (2013).
 - [38] S. D. Mahanti and F. Toigo, *Physics Letters* **36A**, 61 (1971).
 - [39] Phivos Mavropoulos, Private communication.

Supplemental material to “Spin relaxation mechanism in graphene: resonant scattering by magnetic impurities.”

Denis Kochan, Martin Gmitra, and Jaroslav Fabian
*Institute for Theoretical Physics, University of Regensburg,
 93040 Regensburg, Germany*

Details to first-principles calculations.

Density functional theory [1] has been used to calculate the electronic structure of hydrogenated graphene in the supercell approach. We used the generalized gradient approximation for the exchange-correlation functional [2]. The atomic positions in the supercell calculations have been relaxed using the quasi-newton algorithm based on the trust radius procedure implemented within the plane wave pseudopotential code Quantum ESPRESSO [3]. For the atomic species we have used ultra-soft pseudopotentials [4, 5] with PBE exchange-correlation functional [2] with kinetic energies cut-offs of 30 Ry for the wave function and 300 Ry for the density. The vacuum of 15 Å to separate the hydrogenated graphene planes has been used. We found that the covalent C-H bond length d_H is close to 1.13 Å. Next-nearest distance a between the three closest carbon atoms to the hydrogenated carbon, a tetrahedral edge length, is 2.516 Å. The hydrogen bonding distorts the graphene plane by pulling the hydrogenated carbon atom out of plane by about 0.36 Å.

The relaxed structure was then used in the full-potential spin-polarized self-consistent calculations using the linearized augmented plane wave (FLAPW) method as implemented in the FLEUR code [6] in the film mode. We used the cut-off parameter for the plane wave-expansion $k_{\max} = 4.7 \text{ bohr}^{-1}$ and 64 k -points in the irreducible wedge of the Brillouin zone. The muffin-tin radii for carbon of 1.32 bohr and for hydrogen 0.81 bohr were used.

Spin relaxation rate.

The spin relaxation rate is obtained by formulating rate equations. Suppose we have an electron spin accumulation in graphene described by the spin (σ)-dependent chemical potential μ_σ . The electron distribution functions differ from equilibrium as $f_{k\sigma} = f_k^0 + \delta f_{k\sigma}$, where

$$\delta f_{k\sigma} \approx \left(-\frac{\partial f_k^0}{\partial \varepsilon_k} \right) (\mu_\sigma - \varepsilon_F). \quad (1)$$

We denoted as $f_k^0 = f^0(\varepsilon_k)$ the Fermi-Dirac function, ε_k the electron energy, and ε_F the Fermi level. The electron

spin is

$$s = \sum_k \left(-\frac{\partial f_k^0}{\partial \varepsilon_k} \right) \mu_s, \quad (2)$$

with $\mu_s = \mu_\uparrow - \mu_\downarrow$. The spin relaxation rate is defined from equation,

$$\frac{\partial s}{\partial t} = \sum_k \left(-\frac{\partial f_k^0}{\partial \varepsilon_k} \right) \frac{\partial \mu_s}{\partial t} \equiv -\frac{s}{\tau_s}. \quad (3)$$

Let $W_{k\uparrow\downarrow|k'\downarrow\uparrow}$ be the spin-flip rate, that is, the rate of the transition of an electron with momentum k and spin up (\uparrow), in the presence of an impurity with spin down (\downarrow), to another state of momentum k' and spin down (\downarrow), and impurity spin up (\uparrow) (the electron and impurity spins are flipped). Let the probability of the impurity spin being Σ be p_Σ . The rate equation for spin up electrons is

$$\begin{aligned} \frac{\partial f_{k\uparrow}}{\partial t} = & - \sum_{k'} W_{k\uparrow\downarrow|k'\downarrow\uparrow} p_\downarrow f_{k\uparrow} (1 - f_{k'\downarrow}) \\ & + \sum_{k'} W_{k'\downarrow\uparrow|k\uparrow\downarrow} p_\uparrow f_{k'\downarrow} (1 - f_{k\uparrow}). \end{aligned} \quad (4)$$

Assuming unpolarized magnetic moments, $p_\uparrow = p_\downarrow = 1/2$, and using the symmetry of the spin-flip rates, we get

$$\frac{\partial f_{k\uparrow}}{\partial t} = -\frac{1}{2} \sum_{k'} W_{k\uparrow\downarrow|k'\downarrow\uparrow} (f_{k\uparrow} - f_{k'\downarrow}). \quad (5)$$

Similarly for the rate of $f_{k\downarrow}$. We can then write

$$\frac{\partial s}{\partial t} = - \sum_k \sum_{k'} W_{k\uparrow\downarrow|k'\downarrow\uparrow} (\delta f_{k\uparrow} - \delta f_{k'\downarrow}). \quad (6)$$

Substituting the spin accumulation and comparing with the defining equation for τ_s we get

$$\frac{1}{\tau_s} = \frac{\sum_k \sum_{k'} (-\partial f_k^0 / \partial \varepsilon_k) W_{k\uparrow\downarrow|k'\downarrow\uparrow}}{\sum_k (-\partial f_k^0 / \partial \varepsilon_k)}. \quad (7)$$

This equation is used to evaluate the temperature-dependent spin relaxation rates in the paper.

Finally, the transition rates in the presence of N_A impurities are calculated from the T-matrix,

$$W_{k\sigma\Sigma|k'\sigma'\Sigma'} = N_A \frac{2\pi}{\hbar} |T_{k\sigma\Sigma|k'\sigma'\Sigma'}|^2 \delta(\varepsilon_k - \varepsilon_{k'}). \quad (8)$$

All what is necessary for spin-flip rates is to transform the singlet and triplet T-matrix amplitudes, Eq. (5) in the paper, via composite spin states $|\uparrow, \downarrow\rangle$ and $|\downarrow, \uparrow\rangle$. This is a place where the function $f_{\sigma,\sigma'}(x, y)$, Eq. (8) in the main text, enters the game.

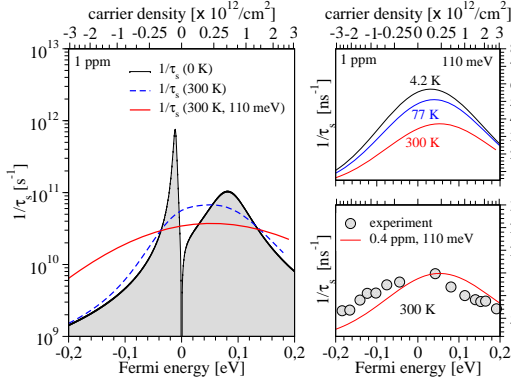


FIG. 1. Same as Fig. 2 of the paper, but with $J = 0.4$ eV. (a) Spin relaxation rate $1/\tau_s$ at zero temperature, at 300 K, and at 300 K and broadened by puddles with 110 meV Dirac point fluctuations. The rates are plotted as functions of energy and (top scale) electron density. The impurity concentration is 1 ppm. (b) Spin relaxation rates, broadened by puddles, at different temperatures. (c) Comparison with experiment, for 0.4 ppm of impurities.

Robustness of spin flip resonant scattering.

In Fig. 1 we show the results for the spin relaxation rates for a ferromagnetic coupling of $J = 0.4$ eV. The singlet and triplet peaks are flipped relative to Fig. 2 of the paper, which is for the antiferromagnetic coupling. Although in a clean system at low temperatures the peaks could be observed, the presence of puddles (or different types of magnetic impurities) wash out the peak structure. The results are quantitatively similar to the antiferromagnetic case, although now the averaged spin relaxation rate is skewed towards positive energies, reflecting the flipped singlet and triplet peaks.

In the paper we claim that the spin relaxation rate is not sensitive to the precise value of J as long as $|J| \gtrsim \Gamma$, where Γ is the resonance width. In Figs. 2, 3, and 4, we plot $1/\tau_s$ and spin-preserving rate $1/\tau$ for exchange couplings $J = -0.04$ eV, $J = -0.004$ eV, and $J = -0.0004$ eV. For $J = -0.04$ eV, the spin relaxation rate for 1 ppm of impurities is still about 100 ps, since at resonance the value of $1/\tau_s$ is unchanged (compared to $J = -0.4$ eV). This lower value of J could also be used to explain the experiment! The singlet and triplet peaks are still resolved. In Fig. 2(b) we plot the ratio of the spin-flip to spin-conserving rates. At resonances, this ratio is about one, meaning that we are still in the regime of $J \gtrsim \Gamma$, and not in the perturbative regime (which is visible outside of the resonance peaks). In Fig. 2(c) we plot the density of states around the Dirac point. The split peak is visible.

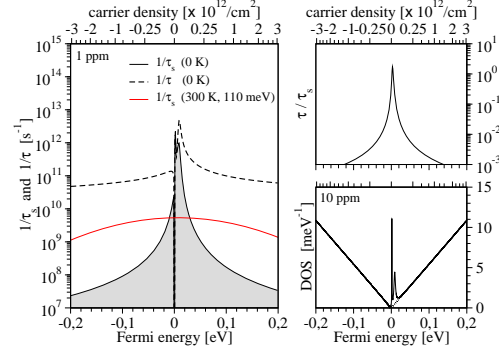


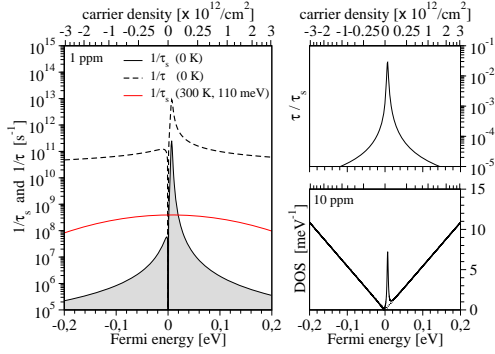
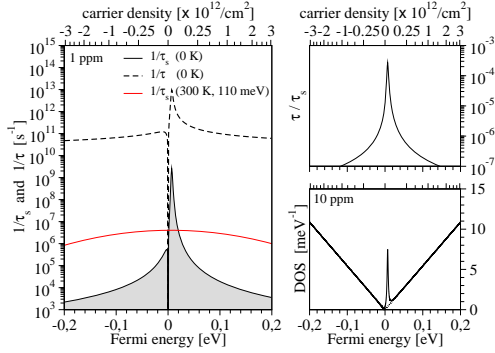
FIG. 2. Spin relaxation rate for $J = -0.04$ eV. (a) Spin relaxation $1/\tau_s$ and spin-preserving $1/\tau$ rates as functions of energy and electron density (top scale). The spin relaxation rate is also shown at 300 K and broadened by puddles with 110 eV energy broadening. The calculations are for 1 ppm impurities. (b) The ratio of the spin-flip and spin-preserving rates. (c) Density of states for 10 ppm of impurities.

If the exchange J further decreases (Γ is of order 10 meV), although the resonance peaks are present, the spin-flip scattering rates become smaller than the spin-preserving rates, as expected from conventional perturbative (Fermi golden rule) scattering. In particular, it is expected that if $J < m\Gamma$, the ratio τ/τ_s decreases as J^2 with decreasing J . This is evident in Figs. 3 and 4. *This is also the regime of spin-orbit coupling.* Say, if an adatom induces local spin-orbit coupling of 1 meV, which is reasonable, then resonance scattering would enhance the spin-orbit spin relaxation rate roughly as $1/16$ ($1/4^2$) compared to what is shown in Fig. 3 (which is for $|J| = 4$ meV). For a 1 ppm of adatoms the spin relaxation time would be 10-100 nanoseconds. The experimental rates could then be achieved by $\eta \approx 10^{-4} - 10^{-3}$ spin-orbit coupling inducing resonant adatoms.

Double-barrier atomic chain with a local moment sitting off the resonant site.

In the paper we state that it is intuitively clear that the exchange coupling on the resonant site dominates spin-flip processes, so we can neglect J on the carbon atoms near hydrogen. We can see this explicitly on our atomic chain model. Suppose a local spin giving exchange J sits not inside resonant well but at one of the barriers, say the left one, i. e. $m = -1$. The model Hamiltonian is as follows:

$$H_{\text{off}} = -t \sum_{\langle m,n \rangle} (c_m^\dagger c_n + c_n^\dagger c_m) + \sum_{m=\mp 1} (U c_m^\dagger c_m - J \delta_{m,-1} \hat{s} \cdot \hat{S}). \quad (9)$$

FIG. 3. Same as in Fig. 2 but for $J = -0.004$ eV.FIG. 4. Same as in Fig. 2 but for $J = -0.0004$ eV.

Transmissions and reflections amplitudes γ_ℓ and β_ℓ can be calculated to be,

$$\gamma_\ell = \frac{-e^{-ikb} + e^{ikb} \mathbb{Y}_\ell}{e^{ikb} + \frac{E_k}{t}(1 + e^{ikb}U/t) + e^{ikb} \mathbb{X}_\ell}, \quad (10)$$

$$\beta_\ell = \gamma_\ell \mathbb{X}_\ell - \mathbb{Y}_\ell, \quad (11)$$

where auxiliary functions \mathbb{X}_ℓ and \mathbb{Y}_ℓ are,

$$\mathbb{X}_\ell = \frac{t + e^{ikb}U}{t + e^{ikb}[U - (4\ell - 3)J]}, \quad (12)$$

$$\mathbb{Y}_\ell = \frac{t + e^{-ikb}[U - (4\ell - 3)J]}{t + e^{ikb}[U - (4\ell - 3)J]}. \quad (13)$$

Figure 5 shows main characteristics of H_{off} , Eq. (9), which allows us to call this model as off-resonant. Panel 5(a) provides the ratio $\mathcal{R}(E)$ for spin-flip *versus*

spin-conserving probabilities, i. e.,

$$\mathcal{R}(E) = [t(E)_{\sigma,-\sigma} + r(E)_{\sigma,-\sigma}] / [t(E)_{\sigma,\sigma} + r(E)_{\sigma,\sigma}] \quad (14)$$

for different J/t . It is obvious when comparing with Fig. 3(a) in the main text that spin-flip processes are

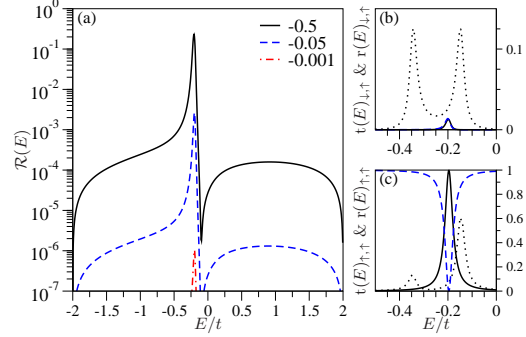


FIG. 5. Atomic chain with a local spin sitting at one of the barriers. (a) Ratio $\mathcal{R}(E)$ of spin-flip versus spin-conserving transition probabilities for $U/t = 10$ and indicated values of J/t . (b) Spin-flip transmission (solid) $t(E)_{\downarrow,\uparrow}$ and reflection (dashed) $r(E)_{\downarrow,\uparrow}$ for $J/t = -0.05$, both magnified by factor 10. (c) Same as in panel (b) but for spin-conserving quantities $t(E)_{\uparrow,\uparrow}$ and $r(E)_{\uparrow,\uparrow}$. For both panels (b) and (c) the dotted lines on the background show corresponding quantities from the resonant model, Eq. (9) in the paper.

significantly suppressed. Figure 5(b) shows transmission and reflection probabilities $t(E)_{\downarrow,\uparrow}$ and $r(E)_{\downarrow,\uparrow}$ for $J/t = -0.05$ (to be visible, they are magnified by factor 10); the dotted line on the background is the transmission probability for the local moment on the resonant site inside the well (see Fig. 3(b) in the main text). Clearly, the spin-flip transitions are much more inhibited than in the resonant case discussed in the paper, justifying neglecting the off-resonant site exchange, especially when energy fluctuations from puddles wash out the fine structure of the resonant peaks. Figure 5(c) shows $t(E)_{\uparrow,\uparrow}$ (solid line) and $r(E)_{\uparrow,\uparrow}$ (dashed line) for $J/t = -0.05$. Similarly, the dotted line represents transmission probability $t(E)_{\uparrow,\uparrow}$ in the resonant case.

-
- [1] J. Hohenberg and W. Kohn, Phys. Rev. **136**, B864 (1964).
 - [2] J. P. Perdew, K. Burke, and M. Ernzerhof, Phys. Rev. Lett. **77**, 3865 (1996).
 - [3] P. Giannozzi and et al., J.Phys.: Condens. Matter **21**, 395502 (2009).
 - [4] D. Vanderbilt, Phys. Rev. B. **41**, 7892 (1990).
 - [5] Source: http://www.quantum-espresso.org/wp-content/uploads/upf_files/C.pbe-van_ak. UPF, http://www.quantum-espresso.org/wp-content/uploads/upf_files/H.pbe-van_ak.UPF.
 - [6] See <http://www.flapw.de/>.